Characterization of Vegetation Loss and Impact on Network Performance at V-Band Frequencies

Brecht De Beelde , David Plets , *Member, IEEE*, and Wout Joseph , *Senior Member, IEEE*

Abstract—**Wireless communication systems using millimeter-wave (mmWave) frequencies can be used for high-throughput applications such as fixed wireless access, where static line-of-sight links are used to provide internet connectivity. The directive antennas are typically mounted on building facades above street level. Therefore, the wireless links are mainly subject to attenuation due to atmospheric absorption, rain, and vegetation. In this letter, we present vegetation loss measurements at V-band frequencies ranging from 50 to 75 GHz, using a spectrum analyzer-based channel sounder. Existing vegetation models, including the vegetation-dependent exponential decay (VED) model, are validated based on the measured vegetation loss. Furthermore, IEEE 802.11ad transceivers are used for the validation of the vegetation models, and to evaluate the influence of vegetation on the network performance via packet error rate (PER) and throughput measurements.**

Index Terms—**Channel sounding, fixed wireless access, foliage loss, hedge, millimeter-wave (mmWave), modeling, outdoor, tree, V-band, vegetation.**

I. INTRODUCTION

WIRELESS communication systems using millimeter-wave (mmWave) frequencies with large channel bandwidths enable high-throughput applications including fixed wireless access (FWA). In FWA networks, high-gain antennas are mounted above street level and a wireless mesh network provides high-speed internet access as a cheaper alternative to optical fiber networks.

The literature on channel models for outdoor environments at mmWave frequencies is available [1], [2], [3], [4], and mmWave outdoor channel models for FWA applications are presented in [5], [6], [7], and [8]. For the design of wireless communication systems for FWA applications, as well as for link budget calculations, vegetation loss models are required to estimate path loss (PL) when the line-of-sight (LOS) path is obstructed. Existing exponential decay models, including the Weissberger [9], FITU-R [10], and COST235 [11] model, have the generic form of (1) and model vegetation loss L (in dB) as a function of frequency f (in MHz or GHz) and vegetation depth d (in meters)

$$L(f, d) = A f^B d^C. \tag{1}$$

The model parameters A, B, and C are fitted based on measurements for frequencies up to 40 GHz [9], [10], [11]. In [12] and [13], vegetation loss measurements at 39 GHz are presented. In [14], we presented vegetation loss measurements at D-band frequencies, ranging from 110 to 170 GHz, and provided a novel model for estimating vegetation loss as a function of frequency and vegetation characteristics. The vegetation-dependent exponential decay (VED) model from (2) expresses vegetation loss L (in dB) as a function of the plant area index (PAI) p, vegetation depth d (in meters), and frequency f (in GHz) [14]. The PAI is a dimensionless parameter and serves as a metric for the vegetation density

$$L(p, d, f) = A f^B d^C p^D. \tag{2}$$

In this letter, we present vegetation loss measurements at V-band frequencies and the measured vegetation loss is compared with existing vegetation loss models. Furthermore, we performed and analyzed network performance measurements using IEEE 802.11ad transceivers. To the best of the authors' knowledge, it is the first time that vegetation loss measurements are presented that cover the full V-band, and that a network performance estimation based on vegetation models is compared to measurements.

II. METHODOLOGY

We performed angular vegetation loss measurements in three environments with different types of vegetation and cultivation using a spectrum analyzer (SA)-based channel sounder as well as an IEEE 802.11ad platform that is also used for network performance measurements.

A. SA-Based Channel Sounder Design

We use the same SA-based channel sounding approach as in [14]. A signal generator generates a radio frequency (RF) signal in the frequency range 8.3–12.5 GHz that is up-converted to the V-band using a frequency multiplier. A vertically polarized omnidirectional transmitting (TX) antenna with a gain of 3 dBi is connected to the frequency multiplier's rectangular waveguide (WR-15). At the receiving (RX) side, a directional RX horn antenna is connected to a harmonic mixer that down-converts the received signal at V-band frequencies to an intermediate frequency (IF) signal that is analyzed by the SA. The RX horn antenna has an azimuth and elevation half-power beamwidth (HPBW) of $20°$, and a gain of 20 dBi.

The noise figure of the SA's IF port is 3 dB, and the conversion loss of the mixer is 18 dB. The resolution bandwidth of the SA of 100 Hz results in a noise level of -151 dBm. We performed
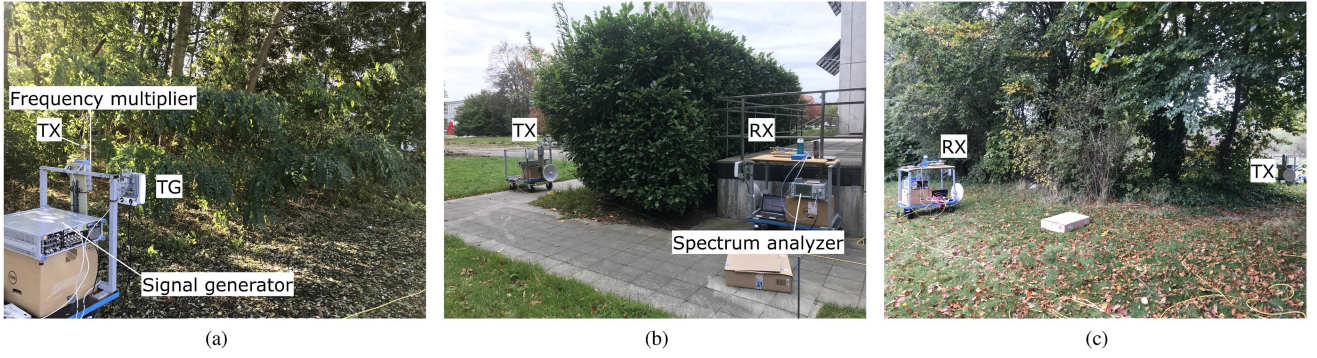
Fig. 1. Measurement environments. (a) Environment 1. (b) Environment 2. (c) Environment 3.

PL measurements for frequencies ranging from 50 to 75 GHz, in steps of 0.5 GHz in different environments and with different antenna separations. With a transmit power of 5 dBm at the antenna input and a total antenna gain of 23 dBi, we can measure PL up to 150 dB.

From the received power, PL (in dB) is calculated via (3), with P_{TX} the transmit power (in dBm), P_{RX} the measured received power (in dBm), G_{TX} and G_{RX} the respective antenna gains of the TX and RX antennas (in dBi), and ϵ a frequency-dependent correction factor (in dB) based on calibration measurements [4], [14]

$$PL = P_{TX} - P_{RX} + G_{TX} + G_{RX} + \epsilon. \quad (3)$$

Both antennas are placed at a height of 1.3 m and leveled horizontally. For each environment and antenna separation, angular PL measurements are performed by rotating the RX antenna in the azimuth plane in steps of 20°, i.e., equal to the RX antenna's HPBW, from −60° to 60°. Angular spread (AS) is calculated via (4), with $P_{RX}(\theta)$ the received power in Watt for azimuth angle θ in radians [15]

$$AS = \frac{180}{\pi} \sqrt{-2\ln\left(\left|\frac{\sum_{\theta \in \Theta} e^{j\theta} P_{RX}(\theta)}{\sum_{\theta \in \Theta} P_{RX}(\theta)}\right|\right)}. \quad (4)$$

B. IEEE 802.11ad Platform

PL and network performance measurements were performed with the Terragraph (TG) channel sounding platform at every location where PL measurements using the SA-based sounder were performed. The TG platform consists of a pair of IEEE 802.11ad-compliant transceivers and is presented in [16]. It is used to perform PL, packet error rate (PER), and throughput measurements for a residential indoor environment in [17]. Each TG node has an antenna array with an HPBW of 2.8°. A phase shifter allows azimuthal beamsteering from −45° to 45° in steps of 1.4°. The effective isotropically radiated power (EIRP) is 38.7 dBm. The center frequency is 60.48 GHz and the channel bandwidth is 2.16 GHz.

The TG platform can be used to measure PL by subtracting received power from the EIRP, and taking into account RF and IF gains. Received power is obtained from received signal strength information and receiver gain settings. Double-directional PL measurements are performed by azimuthal scanning at both TX and RX nodes. An azimuthal scan is also performed prior to the PER and throughput measurements, to select the TX–RX beam combination for which the signal-to-noise ratio is maximal. Using that beam combination, the PER is measured for all modulation and coding scheme (MCS) indices. For the throughput estimation, IEEE 802.11ad waveforms are continuously sent and the proprietary RF baseband algorithm determines the MCS the transceiver would use, based on channel state information embedded in the data frames.

C. Measurement Environments and Scenarios

The different measurement environments are shown in Fig. 1. For each environment, the PAI is determined via a combination of a human estimate and an estimate based on a photograph using the gap light analyzer tool [18]. By changing the location of the antennas, measurements with different vegetation depths are performed. Vegetation depth is defined as the length of the obstructed path. As the antennas are placed outside the vegetation, the vegetation depth is smaller than the antenna separation. Vegetation loss is defined as the excess loss equal to the difference between measured PL, obtained via (3), and the free space PL corresponding to the antenna separation. We obtain the specific attenuation rate in dB per meter by dividing the vegetation loss by the vegetation depth. The tree type of environments 1 and 3 is black locust (*R. pseudoacacia* L). For environment 1, the vegetation depth ranges from 10 to 15 m and the PAI is 2. For environment 3, the vegetation depth ranges from 4.8 to 10.1 m and the PAI is 3.5. The tree type of environment 2 is common laurel (*P. laurocerasus* L.), with a PAI of 9 and a vegetation depth of 3.6 m.

III. VEGETATION LOSS MEASUREMENT RESULTS

Table I lists the measured specific attenuation rate in dB/m of the direct path, i.e., with RX azimuth angle 0°, for the different measurement environments and vegetation depths, as well as the measured AS at 60 GHz. The specific attenuation rate is obtained by measuring vegetation loss with the SA-based channel sounder, averaging over 5GHz sub-bands and normalization with respect to the vegetation depth.
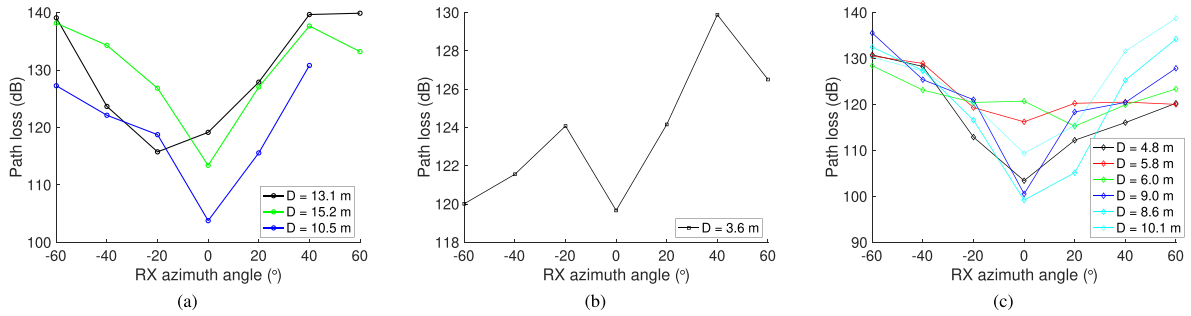
Fig. 2.   Measured PL at 60 GHz as a function of RX azimuth angle for different environments and vegetation depths (D). (a) Environment 1. (b) Environment 2. (c) Environment 3.

TABLE I
AS AT 60 GHz AND SPECIFIC ATTENUATION RATE IN DB/M AT V-BAND
FREQUENCIES FOR DIFFERENT VEGETATION ENVIRONMENTS (E) AND
VEGETATION DEPTHS (D)

| E	D	AS	52.5 GHz	57.5 GHz	62.5 GHz	67.5 GHz	72.5 GHz
1	13.1 m	12°	1.86	1.90	2.11	2.21	2.02
1	15.2 m	9°	1.31	1.21	1.35	1.06	1.53
1	10.5 m	8°	1.06	1.05	0.87	1.17	1.28
2	3.6 m	35°	9.37	10.14	9.21	8.63	9.51
3	4.8 m	14°	3.13	3.02	2.87	2.89	4.43
3	5.8 m	32°	2.59	3.48	3.85	3.96	3.45
3	6.0 m	27°	5.37	5.37	5.10	5.33	4.99
3	9.0 m	6°	1.39	1.53	1.17	1.29	1.29
3	8.6 m	9°	1.01	1.21	1.22	1.27	1.20
3	10.1 m	12°	2.17	2.22	1.75	2.37	1.82
3	9.2 m	17°	3.89	3.43	3.11	3.18	3.18
3	5.1 m	20°	3.75	2.57	3.98	4.03	3.76
3	5.9 m	28°	4.10	4.44	4.96	4.42	5.28
3	6.7 m	6°	1.96	1.52	1.22	1.39	1.82
3	7.8 m	29°	4.03	4.05	4.28	3.66	4.26
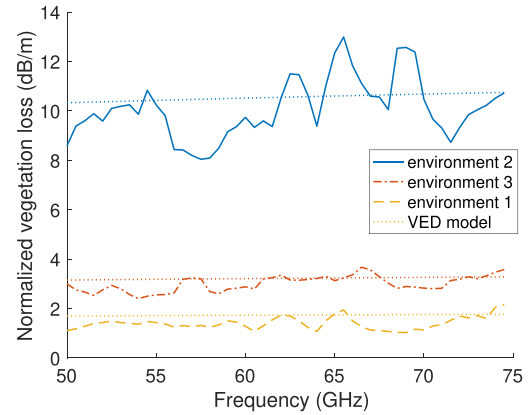
Fig. 3.   Median measured specific attenuation rate as a function of frequency and estimated attenuation using the VED model with d = 1 m for the different vegetation environments.

A. Angular PL

Fig. 2 presents angular PL profiles for the different environments. The minimum PL corresponds to the obstructed direct path, i.e., with the RX antenna directed towards the TX antenna. For all environments, PL for an RX azimuth angle of $\pm 20°$ is only 5–10 dB higher than PL of the direct path. For environment 2, the low PL values that are found for negative RX angles are caused by the environment and not by the vegetation, due to a reflection on nearby objects.

Averaged AS values of about $15°$ are found, which is in line with the values for vertically copolarized measurements reported in [12] and [14]. The angular profiles and high AS confirm that the main propagation mechanism is diffuse scattering, rather than absorption due to tree trunks and foliage.

B. Vegetation Loss

Fig. 3 shows the averaged specific attenuation rate, i.e., vegetation loss divided by the vegetation depth and averaged over the different measurements of the same environment, as a function of frequency for the three measurement environments, based on the PL of the direct path. In line with the Weissberger and FITU-R model, the attenuation increases with increasing frequency, which is not the case for D-band frequencies [14].

The vegetation loss of environment 2 (with common laurel vegetation) is higher than the vegetation loss for environments

1 and 3 (with black locust vegetation). The difference between environments 1 and 3 is explained by the larger average tree diameter, resulting in more absorption. We compare the measured vegetation loss, for the different environments, vegetation depths, and frequencies, to existing models. The root mean squared error (RMSE) between the measured vegetation loss and the COST 235 vegetation model is 10.0 dB. The RMSE between the measurements and the Weissberger model, valid for a vegetation depth up to 14 m, is 11.8 dB. The FITU-R model overestimates vegetation loss considerably, with an RSME of 29.1 dB.

Fitting the measurement data to the exponential decay model from (1) results in parameters $A = 18.9$, $B = 0.2$, and $C = -0.3$. The RMSE is 9.5 dB. Fitting measured vegetation loss to the VED model from (2) results in $A = 0.5$, $B = 0.1$, $C = 0.9$, and $D = 1.2$. The RMSE between the measured PL data and fitted model decreases to 6.1 dB, which is smaller than the RMSE values reported in [12] and [19]. Similar to the VED model at D-band frequencies [14], the regression parameter D was found to be significant at the 5% level, with a p-value below 10^{-3}. In contrast to D-band frequencies, and in line with the Weissberger and FITU-R models, the vegetation loss increases with frequency, resulting in a positive parameter B. The fitted parameters A, B, and C of the VED model at V-band frequencies are close to the parameters of the Weissberger model for vegetation depths up to 14 m. Compared to the VED model
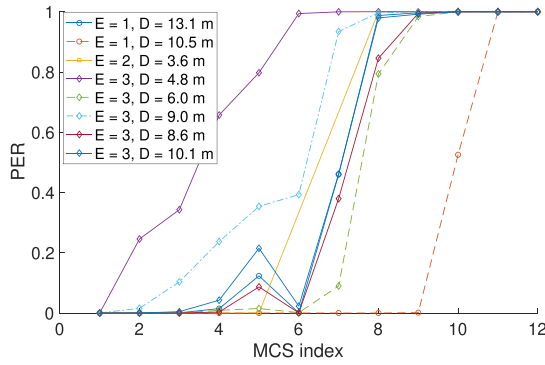
Fig. 4. Measured PER as a function of MCS for different measurement environments (E) and vegetation depths (D).

Fig. 5. Throughput as a function of vegetation depth.

at D-band frequencies, we have an even larger dependence on PAI and a smaller dependence on vegetation depth.

In Section IV, we use a vegetation loss estimation for link budget calculations. Vegetation loss at 60 GHz is estimated via the COST 235 model and VED model with the newly fitted parameters, based on a predefined vegetation depth and PAI. PL is obtained by adding the vegetation loss estimation to the free space PL that corresponds to the antenna separation. The RMSE between the estimated PL and the measured PL of the direct path is 4.6 dB when using the VED model, and 9.9 dB when using the COST 235 model.

IV. MODEL VALIDATION AND NETWORK PERFORMANCE ANALYSIS USING TG PLATFORM

Next to PL measurements with the SA-based channel sounder, we also performed double-directional angular PL measurements with the TG platform, using narrow beamwidth antennas at both TX and RX sides. From the angular PL measurement results, we select the minimum measured PL. The mean difference between the PL measured with the TG platform and the PL at 60 GHz, measured with the SA-based sounder, is 1.6 dB, whereas the RMSE between the two measurements is 9.2 dB. The difference is caused by the difference in antenna beamwidth. Furthermore, beamsteering of the TG platform at both TX and RX allows finding a propagation path through the vegetation with lower PL than the direct path.

Using the TG platform, we also performed PER measurements. Measured PER as a function of the used MCS index is shown in Fig. 4 for the different measurement environments and vegetation depths. The PER for MCS index 6 is below 0.25 for all measurements, except for environment 3 with vegetation depths of 4.8 and 9.0 m. Only for environment 1 and the smallest vegetation depth of 10.5 m (with an antenna separation of 14.9 m) can an MCS index of 9 be used.

Finally, the TG platform is used to perform throughput measurements, based on the adaptive rate control algorithm implementation of the RF transceiver. The throughput measurements are compared to throughput estimations via a link budget analysis. In the link budget calculation, received power levels are obtained by subtracting measured and estimated PL from an
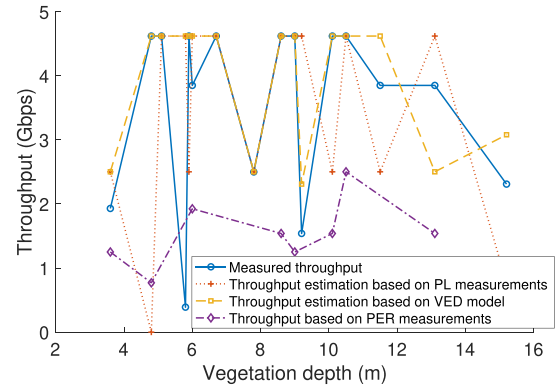
EIRP of 38.7 dBm, which is the EIRP used by the TG platform. The gain of the RX antenna is 25 dBi. Received power should be higher than the receiver sensitivity using a certain MCS [20]. The estimated and measured throughputs as a function of vegetation depth are shown in Fig. 5. This figure also shows a throughput estimation based on PER measurements, i.e., the throughput corresponding to the MCS for which the measured PER is below 0.25. For all measurement scenarios, the estimation using the MCS selection based on PER measurements estimates a lower throughput compared to the measured and estimated throughput. Based on the link budget calculations, MCS indices 10 and higher can be used, which is higher than the MCS indices that are obtained via PER measurements. The high PER was also reported in [17] and might be related to other RF impairments of the TG platform.

V. CONCLUSION

In this letter, the results and analysis of vegetation loss measurements at V-band frequencies are presented to characterize signal attenuation in a vegetated environment for FWA applications. Azimuthal AS values range from 6° to 35°, and the COST 235 vegetation loss model gives a good fit to the measurement data, with an RMSE of 10 dB. Fitting the measurement data to an exponential decay model results in a similar RMSE of 9.5 dB. The RMSE decreases to 6.1 dB if we fit the measurement data to the VED model, which takes into account the vegetation density. Throughput estimations based on link budget calculations using estimated or measured PL return higher values compared to throughput measurements using the TG platform. The PER measurements show that the throughput estimations and measurements provide an upper bound, as the PER measurements using the MCS values from the throughput measurements return PER values above 50%.

REFERENCES

[1] X. Zhao, S. Li, Q. Wang, M. Wang, S. Sun, and W. Hong, "Channel measurements, modeling, simulation and validation at 32 GHz in outdoor microcells for 5G radio systems," *IEEE Access*, vol. 5, pp. 1062–1072, 2017.

[2] J. Lee, K.-W. Kim, M.-D. Kim, J.-J. Park, Y. K. Yoon, and Y. J. Chong, "Measurement-based millimeter-wave angular and delay dispersion characteristics of outdoor-to-indoor propagation for 5G millimeter-wave systems," *IEEE Access*, vol. 7, pp. 150492–150504, 2019.

[3] S. H. A. Momo and M. M. Mowla, "Statistical analysis of an outdoor mmwave channel model at 73 GHz for 5G networks," in *Proc. IEEE Int. Conf. Comput., Commun., Chem., Mater. Electron. Eng.*, 2019, pp. 1–4.

[4] B. De Beelde, E. Tanghe, D. Plets, and W. Joseph, "Outdoor line-of-sight path loss modeling at 140 GHz," in *Proc. IEEE 16th Eur. Conf. Antennas Propag.*, 2022, pp. 1–4.

[5] G. R. MacCartney and T. S. Rappaport, "73 GHz millimeter wave propagation measurements for outdoor urban mobile and backhaul communications in new york city," in *Proc. IEEE Int. Conf. Commun.*, 2014, pp. 4862–4867.

[6] Y. Xing and T. S. Rappaport, "Millimeter wave and terahertz urban microcell propagation measurements and models," *IEEE Commun. Lett.*, vol. 25, no. 12, pp. 3755–3759, Dec. 2021.

[7] D. Dupleich et al., "Multi-band propagation and radio channel characterization in street canyon scenarios for 5G and beyond," *IEEE Access*, vol. 7, pp. 160385–160396, 2019.

[8] B. De Beelde, E. Tanghe, D. Plets, and W. Joseph, "Outdoor channel modeling at D-band frequencies for future fixed wireless access applications," *IEEE Wireless Commun. Lett.*, vol. 11, no. 11, pp. 2355–2359, Nov. 2022, doi: 10.1109/LWC.2022.3202921.

[9] M. A. Weissberger, "An initial critical summary of models for predicting the attenuation of radio waves by trees," Electromagnetic Compatibility Analysis Center, Annapolis, MD, USA, Tech. Rep. ESD-TR-81-101, 1982.

[10] M. Al-Nuaimi and R. Stephens, "Measurements and prediction model optimisation for signal attenuation in vegetation media at centimetre wave frequencies," *IEEE Proc. - Microw. Antennas Propag.*, vol. 145, pp. 201–206, Jun. 1998. [Online]. Available: https://digital-library.theiet.org/content/journals/10.1049/ip-map_19981883

[11] G. Dooren, H. van Govaerts, and M. Herben, *COST 235: Radiowave Propagation Effects on Next-Generation Fixed-Services Terrestrial Telecommunications Systems*. Technische Universiteit Eindhoven, Eindhoven, The Netherlands, 1997.

[12] Y. Lv, X. Yin, C. Zhang, and H. Wang, "Measurement-based characterization of 39 GHz millimeter-wave dual-polarized channel under foliage loss impact," *IEEE Access*, vol. 7, pp. 151558–151568, 2019.

[13] P. Zhang, B. Yang, C. Yi, H. Wang, and X. You, "Measurement-based 5G millimeter-wave propagation characterization in vegetated suburban macrocell environments," *IEEE Trans. Antennas Propag.*, vol. 68, no. 7, pp. 5556–5567, Jul. 2020.

[14] B. De Beelde, R. De Beelde, E. Tanghe, D. Plets, K. Verheyen, and W. Joseph, "Vegetation loss at D-band frequencies and new vegetation-dependent exponential decay model," *IEEE Trans. Antennas Propag.*, early access, 2022, doi: 10.1109/TAP.2022.3209215.

[15] 3GPP, "Study on channel model for frequencies from 0.5 to 100 GHz," 3rd Generation Partnership Project (3GPP), Sophia Antipolis, France, Tech. Rep. (TR) 38.901, 2017.

[16] A. Shkel, A. Mehrabani, and J. Kusuma, "A configurable 60 GHz phased array platform for multi-link mmwave channel characterization," in *Proc. IEEE Int. Conf. Commun. Workshops*, 2021, pp. 1–6.

[17] B. De Beelde, A. Almarcha, D. Plets, and W. Joseph, "V-band channel modeling, throughput measurements, and coverage prediction for indoor residential environments," *Electronics*, vol. 11, no. 4, 2022, Art. no. 659. [Online]. Available: https://www.mdpi.com/2079-9292/11/4/659

[18] G. Frazer, C. Canham, and K. Lertzman, *Gap Light Analyzer (GLA): Imaging Software to Extract Canopy Structure and Gap Light Transmission Indices From True-Colour Fisheye Photographs*, Simon Fraser University, Burnaby, BC, Canada, The Institute of Ecosystem Studies, Millbrook, NY, USA, 1999.

[19] Y. Zhang, C. R. Anderson, N. Michelusi, D. J. Love, K. R. Baker, and J. V. Krogmeier, "Propagation modeling through foliage in a coniferous forest at 28 GHz," *IEEE Wireless Commun. Lett.*, vol. 8, no. 3, pp. 901–904, Jun. 2019.

[20] *IEEE Standard for Information Technology—Telecommunications and Information Exchange Between Systems—Local and Metropolitan Area Networks-Specific Requirements—Part 11: Wireless LAN Medium Access Control (MAC) and Physical Layer (PHY) Specifications Amendment 3: Enhancements for Very High Throughput in the 60 GHz Band*, IEEE 802.11ad, 2012.